ARCHIVES OF ELECTRICAL ENGINEERING VOL. 71(4), pp. 1081 –1106 (2022)

DOI 10.24425/aee.2022.142126

Solution of nonlinear stiff differential equations for a three-phase no-load transformer using a Runge–Kutta implicit method

BERNARD BARON[1], JOANNA KOLAŃSKA-PŁUSKA[1] ✉, MARIAN ŁUKANISZYN[1], DARIUSZ SPAŁEK[2], TOMASZ KRASZEWSKI[3]

[1] *Faculty of Electrical Engineering, Automatic Control and Informatics, Opole University of Technology Prószkowska 76, 45-758 Opole, Poland*

[2] *Institute of Electrotechnics and Informatics, Silesian University of Technology 10 Akademicka St., 44-100 Gliwice, Poland*

[3] *Research and Development Center GLOKOR Sp. z o.o. Górnych Wałów 27A St., 44-100 Gliwice, Poland*

e-mail: {b.baron/✉j.kolanska-pluska/m.lukaniszyn}@po.edu.pl, dariusz.spalek@polsl.pl, t.kraszewski@glokor.eu

(Received: 04.07.2022, revised: 17.10.2022)

Abstract: The paper presents an approach to differential equation solutions for the stiff problem. The method of using the classic transformer model to study nonlinear steady states and to determine the current pulses appearing when the transformer is turned on is given. Moreover, the stiffness of nonlinear ordinary differential state equations has to be considered. This paper compares Runge–Kutta implicit methods for the solution of this stiff problem.

Key words: circuit model of a three-phase transformer, Runge–Kutta implicit methods, stiff nonlinear ordinary differential equations

1. Introduction

At present, Runge–Kutta methods are commonly used for the solution of ordinary differential equations [5,6,16], partial differential equations [14,15], and integral equations [17]. The implicit Runge–Kutta algorithms are applied for transient state analysis of electromagnetic problems [13–15,18].

The present work is a continuation of the work by the authors [3] that concerned the modeling of current pulses when supplying an unloaded single-phase transformer. The current paper presents approaches to the numerical analysis of differential states equations that describe transient states of a nonlinear transformer at a no-load state of work [7–9,19,21]. The monograph [11] presents the numerical analysis of the magnetic field that occurs around the transformer after it has been switched off. The purpose of this analysis was to determine if it is possible to define the residual fluxes in the legs of the transformer based on the measurements of this field. These studies have allowed us to determine the quantity and location of the sensors. The influence of the Earth's magnetic field has also been studied. In these works [10,11] also on the basis of description inrush current, the influence of residual magnetism has been determined. Residual flux in the legs was considered as an initial condition. Nowadays, an increase in the maximal magnetic flux density of the transformer core results in a decrease in dimensions. As a physical consequence, the magnetizing current decreases. A mathematical consequence appears while the transformer circuit model is being derived. The differential equations become stiffer and stiffer. Further consequences are as follows: impulse inrush currents appear and insulation tension significantly increases as the transformer is being switched on. In order to calculate values of both dangerous phenomena, the stiff nonlinear ordinary differential equations for the transformer circuit model have to be solved. For this purpose, Runge–Kutta implicit methods are derived [1–4,7]. This paper also presents a comparison of proposed methods for the solution of the stiff problem considered.

Anisotropic transformer sheets are characterized by a narrow hysteresis loop and a relatively low residual magnetism associated with an increase in the maximum allowable magnetic induction. This problem can also be solved by using field methods considering anisotropy and hysteresis [17,21]. However, according to the authors, proposing an approach based on circuit methods is effective and allows for faster results.

2. Nonlinear model of a three-phase transformer with a nonlinear magnetizing curve

The three-phase transformer (primary winding star-connected) considered is described by circuit differential equations. The three-phase transformer equations are derived based on the well-known transformer circuit model as shown in Fig. 1.

The H-B curve for transformer steel is given by polynomial $H_S(B)$ of 11^{th} degree in the following form:

$$H_S(B) = \sum_{k=1}^{11} a_k B^{2k-1}, \tag{1}$$

and is graphically presented in Fig. 2.

Operating solely with characteristics, however, does not allow for the inclusion of loss of iron in modeling (due to over magnetization and eddy currents). For this purpose, a dynamic term proportional to the induction derivative B with constant is added to the unambiguous characteristic (1):

$$H(B) = H_S(B) + k_B \frac{\mathrm{d}B}{\mathrm{d}t}. \tag{2}$$

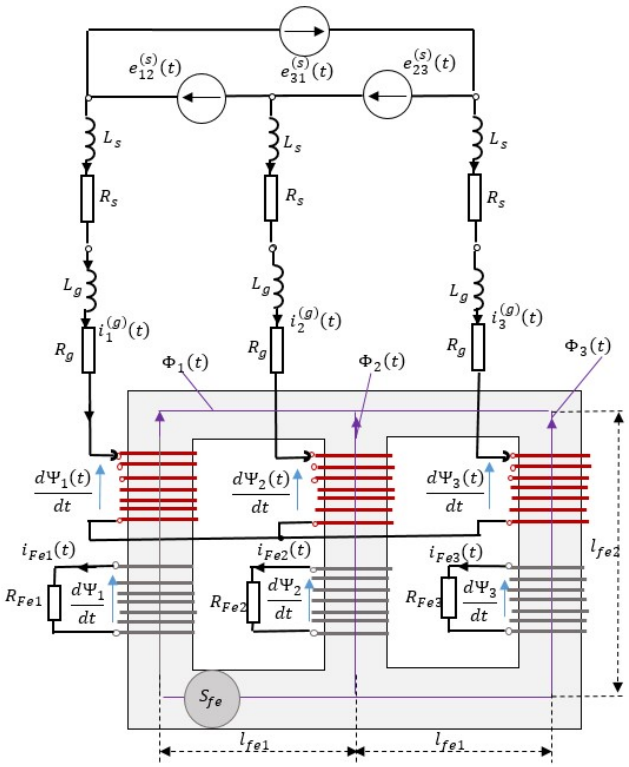

Fig. 1. Three-phase transformer equivalent circuit

Nomenclature:

z_g	coil number of high voltage winding (equal for each winding)
l_{Fe1}, l_{Fe2}	average length of transformer column and yoke, respectively
S_{Fe}	cross-section of transformer core
$R_{\mathrm{Fe},k}$	resistances representing core power losses
L_g	leakage inductance for high voltage winding
R_g	resistance for high voltage winding
L_s	source inductance
R_s	source resistance
$\Psi_k(t)$	flux linkages of primary windings for $k = 1, 2, 3$
$\Phi_k(t)$	flux of k-th magnetic circuit column for $k = 1, 2, 3$
$i_k^{(g)}(t)$	current of primary k-th winding for $k = 1, 2, 3$
$i_{\mathrm{Fe},k}(t)$	current no-load component at resistance on equivalent z_g coils
$e_{12}^{(s)}(t)$	source voltages: $e_{12}^{(s)}(t) = E_{m_{12}} \cos\left(\omega t - \frac{\pi}{6} + \varphi_0\right)$,
$e_{23}^{(s)}(t)$	$e_{23}^{(s)}(t) = E_{m_{23}} \cos\left(\omega t + \frac{\pi}{2} + \varphi_0\right)$,
$e_{31}^{(s)}(t)$	$e_{31}^{(s)}(t) = E_{m_{31}} \cos\left(\omega t + \frac{7\pi}{6} + \varphi_0\right)$
ϕ_0	initial phase

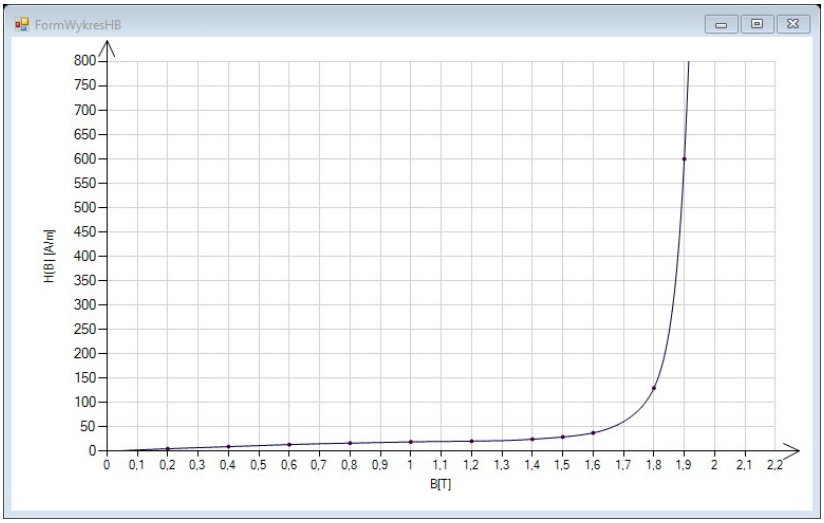

Fig. 2. Magnetizing curve for transformer steel of the type Power Core H 105-30 (Thyssen Krupp Elektrical Steel)

The magnetic voltage drop in the kth transformer column is approximately in the form of

$$\widetilde{U}_{m,k}\left(\Psi_k(t)\right) = h_{\mathrm{Fe},k} H\left(\frac{\Psi_k(t)}{z_g S_{\mathrm{Fe}}}\right) = h_{\mathrm{Fe},k} H_S\left(\frac{\Psi_k(t)}{z_g S_{\mathrm{Fe}}}\right) + \frac{h_{\mathrm{Fe},k} k_{B,k}}{z_g S_{\mathrm{Fe}}} \frac{\mathrm{d}\Psi_k(t)}{\mathrm{d}t}, \tag{3}$$

where $h_{\mathrm{Fe},k}$ is the average length of the k-th branch of the transformer's magnetic circuit and $k = 1, 2, 3$.

It can be assumed that the flux derivative $\dfrac{\mathrm{d}\Psi_k(t)}{\mathrm{d}t}$ appearing in this equation is the electromotive force of induction on the terminals of a coil with z_g coils with zero resistance wound on the k-th transformer column, which is short-circuited with resistance $R_{\mathrm{Fe},k}$ (Fig. 1).

$$\frac{\mathrm{d}\Psi_k(t)}{\mathrm{d}t} = R_{\mathrm{Fe},k} i_{\mathrm{Fe},k}(t), \tag{4}$$

where $i_{\mathrm{Fe},k}$ is the current of this coil.

In such a circuit modelling of the transformer's magnetic circuit, the second term of the magnetic voltage drop can be expressed in Formula (3) $\dfrac{h_{\mathrm{Fe},k} k_{B,k}}{z_g S_{\mathrm{Fe}}} \dfrac{\mathrm{d}\Psi_k(t)}{\mathrm{d}t}$ by the additional magnetomotor force $z_g i_{\mathrm{Fe},k}(t)$ expressed by Formula (5):

$$z_g i_{\mathrm{Fe},k}(t) = \frac{h_{\mathrm{Fe},k} k_{B,k}}{z_g S_{\mathrm{Fe}}} \frac{\mathrm{d}\Psi_k(t)}{\mathrm{d}t}, \qquad \text{where } k = 1, 2, 3. \tag{5}$$

From Eq. (5) it follows that the constant $k_{B,k}$ is given by the formula:

$$k_{B,k} = \frac{(z_g)^2 S_{\mathrm{Fe}}}{h_{\mathrm{Fe},k} R_{\mathrm{Fe},k}}, \qquad \text{where } k = 1, 2, 3. \tag{6}$$

The parameters $R_{\mathrm{Fe},k}$ in the model can be determined from the measurement of the transformer's active power an no load state of work. Such a mathematical model of the transformer can therefore be used to determine the state established as a limit cycle of the solution of the relevant differential equations, which will be shown in the following points. The given mathematical model does not take into account magnetic hysteresis because it does not follow the "history" of magnetization of the core, i.e. the points at which the directions of changes in currents and magnetic fluxes are reversed. The history of magnetization of the core can be known at the time of switching the transformer to the network in the form of residual magnetism. So, if we know the residual magnetism of the transformer, we have the possibility of setting initial conditions for state variables $\Psi_1(t_0)$, $\Psi_2(t_0)$ which are coupled fluxes. As you know (e.g. [10, 11]), when the transformer is connected to the network, current pulses many times higher than the rated values appear in the first voltage period. So, if the analysis of the transient state of the transformer is limited to the first period, the use of the proposed model with initial conditions allows to study the influence of the values of these current pulses depending on the residual magnetism. Physically speaking, current pulses appear at the first entry into the area of saturation of the core. Therefore, in addition to taking into account residual magnetism in modeling, accurate approximation in the magnetization characteristics in the saturation area should be used. This article uses the odd-numbered polynomial (1). In the construction of the mathematical model of the transformer, the magnetomotor forces generated by the currents of the coils $i_k^{(g)}(t)$ $(k = 1, 2, 3)$ should be supplemented by magneto motor forces generated by certain substitute currents $i_{\mathrm{Fe},k}(t)$ corresponding to power losses in the core and expressed in the form of $z_g i_{\mathrm{Fe},k}(t)$.

The magnetomotive forces for the no-load state of work $\theta_k(t)$ for $k = 1, 2, 3$ are given by the relations as follows for three transformers column.

$$\theta_k(t) = z_g \left(i_k^{(g)}(t) - i_{\mathrm{Fe},k}(t) \right). \tag{7}$$

For nonlinear magnetic circuit voltage Kirchhoff's law lead to the following equation set:

$$\begin{bmatrix} \theta_1(t) - U_{\mu,1}(\Psi_1(t)) - \theta_2(t) + U_{\mu,2}(\Psi_2(t)) \\ \theta_2(t) - U_{\mu,2}(\Psi_2(t)) - \theta_3(t) + U_{\mu,3}(\Psi_3(t)) \end{bmatrix} = 0, \tag{8}$$

where $\Psi_k(t) = z_g \Phi_k(t)$, $h_{\mathrm{Fe},k}$ means average length of k-th phase magnetic circuit and

$$U_{\mu,k}(\Psi_k(t)) = \frac{h_{\mathrm{Fe},k} H(\Psi_k(t))}{(z_g S_{\mathrm{Fe}})} \tag{9}$$

denotes magnetic voltage drop for the k-th phase.

Equations (7) and (8) lead to the following relation:

$$\begin{bmatrix} \begin{bmatrix} i_1^{(g)}(t) - i_{\mathrm{Fe1}}(t) \end{bmatrix} z_g - \begin{bmatrix} i_2^{(g)}(t) - i_{\mathrm{Fe2}}(t) \end{bmatrix} z_g \\ \begin{bmatrix} i_2^{(g)}(t) - i_{\mathrm{Fe2}}(t) \end{bmatrix} z_g - \begin{bmatrix} i_3^{(g)}(t) - i_{\mathrm{Fe3}}(t) \end{bmatrix} z_g \end{bmatrix} = \begin{bmatrix} U_{\mu,1}(\Psi_1(t)) - U_{\mu,2}(\Psi_2(t)) \\ U_{\mu,2}(\Psi_2(t)) - U_{\mu,3}(\Psi_3(t)) \end{bmatrix}, \tag{10}$$

where equivalent currents $i_{\mathrm{Fe},k}(t)$ model the power losses in the ferromagnetic core of the transformer. After putting the currents $i_{\mathrm{Fe},k}(t)$ from the relation

$$\frac{\mathrm{d}\Psi_k(t)}{\mathrm{d}t} = z_g \frac{\mathrm{d}\Phi_k(t)}{\mathrm{d}t} = R_{\mathrm{Fe},k} i_{\mathrm{Fe},k}(t) \tag{11}$$

into Eq. (10), it can be rewritten as follows:

$$\left[i_1^{(g)}(t) - \frac{1}{R_{\mathrm{Fe}1}}\frac{\mathrm{d}\Psi_1(t)}{\mathrm{d}t}\right] z_g - \left[i_2^{(g)}(t) - \frac{1}{R_{\mathrm{Fe}2}}\frac{\mathrm{d}\Psi_2(t)}{\mathrm{d}t}\right] z_g = U_{\mu,1}(\Psi_1(t)) - U_{\mu,2}(\Psi_2(t)), \quad (12)$$

$$\left[i_2^{(g)}(t) - \frac{1}{R_{\mathrm{Fe}2}}\frac{\mathrm{d}\Psi_2(t)}{\mathrm{d}t}\right] z_g - \left[i_3^{(g)}(t) - \frac{1}{R_{\mathrm{Fe}3}}\frac{\mathrm{d}\Psi_3(t)}{\mathrm{d}t}\right] z_g = U_{\mu,2}(\Psi_2(t)) - U_{\mu,3}(\Psi_3(t)). \quad (13)$$

Current Kirchhoff's laws for both fluxes linkages and phase currents take the following forms:

$$\Psi_1(t) + \Psi_2(t) + \Psi_3(t) = 0, \quad (14)$$

$$i_1^{(g)}(t) + i_2^{(g)}(t) + i_3^{(g)}(t) = 0, \quad (15)$$

which enable (12) and (13) to be rewritten as follows:

$$\frac{1}{R_{\mathrm{Fe}1}}\frac{\mathrm{d}\Psi_1(t)}{\mathrm{d}t} - \frac{1}{R_{\mathrm{Fe}2}}\frac{\mathrm{d}\Psi_2(t)}{\mathrm{d}t} = i_1^{(g)}(t) - i_2^{(g)}(t) - z_g^{-1}U_{\mu,1}(\Psi_1(t)) + z_g^{-1}U_{\mu,2}(\Psi_2(t)) \equiv h_3(\boldsymbol{X}), \quad (16)$$

$$\begin{aligned}\frac{1}{R_{\mathrm{Fe}3}}\frac{\mathrm{d}\Psi_1(t)}{\mathrm{d}t} + \left(\frac{1}{R_{\mathrm{Fe}2}} + \frac{1}{R_{\mathrm{Fe}3}}\right)\frac{\mathrm{d}\Psi_2(t)}{\mathrm{d}t} \\ = i_1^{(g)}(t) + 2i_2^{(g)}(t) - z_g^{-1}U_{\mu,2}(\Psi_2(t)) + z_g^{-1}U_{\mu,3}(-\Psi_1(t) - \Psi_2(t)) \equiv h_4(\boldsymbol{X}),\end{aligned} \quad (17)$$

where state vector $\boldsymbol{X} = [x_1(t), x_2(t), x_3(t), x_4(t)]^T$ is defined. Equations (16) and (17) can be solved with respect to derivatives of the states of the variables $x_3 \equiv \Psi_1(t)$ and $x_4 \equiv \Psi_2(t)$, and thus the following matrix form is obtained:

$$\begin{bmatrix}\frac{\mathrm{d}x_3(t)}{\mathrm{d}t} \\ \frac{\mathrm{d}x_4(t)}{\mathrm{d}t}\end{bmatrix} = \begin{bmatrix}\frac{\mathrm{d}\Psi_1(t)}{\mathrm{d}t} \\ \frac{\mathrm{d}\Psi_2(t)}{\mathrm{d}t}\end{bmatrix} = \boldsymbol{G}^{-1}\begin{bmatrix}h_3(\boldsymbol{X}) \\ h_4(\boldsymbol{X})\end{bmatrix} = \begin{bmatrix}r_{11} & r_{12} \\ r_{21} & r_{22}\end{bmatrix}\begin{bmatrix}h_3(\boldsymbol{X}) \\ h_4(\boldsymbol{X})\end{bmatrix} \equiv \begin{bmatrix}f_3(\boldsymbol{X}) \\ f_4(\boldsymbol{X})\end{bmatrix}, \quad (18)$$

where it is denoted as

$$\boldsymbol{G} = \begin{bmatrix}\frac{1}{R_{\mathrm{Fe}1}} & \frac{-1}{R_{\mathrm{Fe}2}} \\ \frac{1}{R_{\mathrm{Fe}3}} & \frac{1}{R_{\mathrm{Fe}2}} + \frac{1}{R_{\mathrm{Fe}3}}\end{bmatrix}, \qquad \boldsymbol{G} = \begin{bmatrix}r_{11} & r_{12} \\ r_{21} & r_{22}\end{bmatrix}^{-1},$$

$$r_{11} = \frac{1}{\frac{1}{R_{\mathrm{Fe}1}} + \frac{1}{R_{\mathrm{Fe}2} + R_{\mathrm{Fe}3}}}, \qquad r_{12} = \frac{1}{\frac{1}{R_{\mathrm{Fe}1}} + \frac{R_{\mathrm{Fe}2}}{R_{\mathrm{Fe}1}R_{\mathrm{Fe}3}} + \frac{1}{R_{\mathrm{Fe}3}}},$$

$$r_{21} = \frac{-1}{\frac{R_{\mathrm{Fe}3}}{R_{\mathrm{Fe}1}R_{\mathrm{Fe}2}} + \frac{1}{R_{\mathrm{Fe}1}} + \frac{1}{R_{\mathrm{Fe}2}}}, \qquad r_{22} = \frac{1}{\frac{1}{R_{\mathrm{Fe}2}} + \frac{1}{R_{\mathrm{Fe}3}} + \frac{R_{\mathrm{Fe}1}}{R_{\mathrm{Fe}2}R_{\mathrm{Fe}3}}}.$$

Voltage Kirchhoff's law for two independent circuits of primary transformer windings leads to two independent relations

$$L_z\frac{\mathrm{d}i_1^{(g)}(t)}{\mathrm{d}t} + R_z i_1^{(g)}(t) + \frac{\mathrm{d}\Psi_1(t)}{\mathrm{d}t} - L_z\frac{\mathrm{d}i_2^{(g)}(t)}{\mathrm{d}t} - R_z i_2^{(g)}(t) - \frac{\mathrm{d}\Psi_2(t)}{\mathrm{d}t} = e_{12}^{(s)}(t), \quad (19)$$

$$L_z \frac{\mathrm{d}i_2^{(g)}(t)}{\mathrm{d}t} + R_z i_2^{(g)}(t) + \frac{\mathrm{d}\Psi_2(t)}{\mathrm{d}t} - L_z \frac{\mathrm{d}i_3^{(g)}(t)}{\mathrm{d}t} - R_z i_3^{(g)}(t) - \frac{\mathrm{d}\Psi_3(t)}{\mathrm{d}t} = e_{23}^{(s)}(t), \tag{20}$$

which can be written in matrix notation as follows:

$$\begin{bmatrix} L_z & -L_z \\ L_z & 2L_z \end{bmatrix} \begin{bmatrix} \dfrac{\mathrm{d}i_1^{(g)}(t)}{\mathrm{d}t} \\ \dfrac{\mathrm{d}i_2^{(g)}(t)}{\mathrm{d}t} \end{bmatrix} = \begin{bmatrix} h_1(\boldsymbol{X}) \\ h_2(\boldsymbol{X}) \end{bmatrix}, \tag{21}$$

where

$$h_1(\boldsymbol{X}) = e_{12}^{(s)}(t) - R_z i_1^{(g)}(t) + R_z i_2^{(g)}(t) - f_3(\boldsymbol{X}) + f_4(\boldsymbol{X}),$$
$$h_2(\boldsymbol{X}) = e_{23}^{(s)}(t) - R_z i_1^{(g)}(t) - 2R_z i_2^{(g)}(t) - f_3(\boldsymbol{X}) - 2f_4(\boldsymbol{X}).$$

The solutions of Eq. (21) with respect to current derivatives are as follows:

$$\begin{bmatrix} \dfrac{\mathrm{d}x_1(t)}{\mathrm{d}t} \\ \dfrac{\mathrm{d}x_2(t)}{\mathrm{d}t} \end{bmatrix} \equiv \begin{bmatrix} \dfrac{\mathrm{d}i_1^{(g)}(t)}{\mathrm{d}t} \\ \dfrac{\mathrm{d}i_2^{(g)}(t)}{\mathrm{d}t} \end{bmatrix} = \frac{1}{2L_z} \begin{bmatrix} 2h_1(\boldsymbol{X}) + h_2(\boldsymbol{X}) \\ -h_1(\boldsymbol{X}) + h_2(\boldsymbol{X}) \end{bmatrix} \equiv \begin{bmatrix} f_1(\boldsymbol{X}) \\ f_2(\boldsymbol{X}) \end{bmatrix}. \tag{22}$$

Equations (18) and (22) constitute the differential state equation set for the state vector $\boldsymbol{X} = [x_1(t), x_2(t), x_3(t), x_4(t)]^T$, and describe the no-load state of work of the transformer where primary windings are star-connected (Fig. 4(a)). The resulting system of Eqs. (18) and (22) does not take into account magnetic hysteresis in general and the question arises with what simplifications we are dealing with when applying it. This model is used to study the steady states of the transformer if the resistance $R_{\mathrm{Fe},k}$ is determined based on the idle losses of the transformer, which take into account eddy currents and magnetic hysteresis. Starting from any initial conditions (e.g. zero) of the system of Eqs. (18) and (22) we will reach a steady state that is the limit cycle of this solution. The result of this integration can be verified by simple metrological techniques. For this type of issue, in the article below, a special algorithm has been developed for determining such initial conditions for which, despite the high rigidity of these equations, the total calculation cost is the smallest possible (point 5). The trajectories of the transition to this boundary cycle do not have a physical interpretation in this case. As mentioned, the given mathematical model does not take into account magnetic hysteresis because it does not track the "history" of magnetization of the core, i.e. the points at which the directions of changes in currents and magnetic fluxes are reversed. The history of magnetization of the core can be known at the time of switching the transformer to the network in the form of residual magnetism. So we have the ability to set initial conditions for state variables $\Psi_1(t_0)$, $\Psi_2(t_0)$ that are conjugate streams $\Psi_1(t_0) = B_1 S_{\mathrm{Fe}} z_g$, $\Psi_2(t_0) = B_2 S_{\mathrm{Fe}} z_g$ where B_1, B_2 are the residual induction of transformer cores. By performing integration under such initial conditions, the first input into the core saturation area for which the largest current pulses are obtained gives an accurate solution. Therefore, the article conducts research on the effect of residual magnetism on the maximum values of the transformer current in the first period of supply voltage. Studies were also carried out to determine the influence of the $R_{\mathrm{Fe},k}$ parameter of the model on the maximum value of current pulses when switching on the voltage. Studies have shown that the change in total losses in iron per unit volume given by the

manufacturer of transformer sheets within the wide limits on the basis of which this parameter is determined does not have a significant impact on the maximum values of currents obtained from solving the mathematical model. Therefore, the developed model can be successfully used to test the steady state of the transformer and to calculate the maximum current pulses when the transformer is connected to the network.

3. Application of implicit Runge–Kutta methods

The paper proposes to apply Runge–Kutta implicit methods for the solution of the differential set obtained in paragraph #2. The general form of Runge–Kutta implicit methods has the form of:

$$\boldsymbol{X}_{i+1} = \boldsymbol{X}_i + \sum_{j=1}^{m} w_j \boldsymbol{K}_j^{(i)}, \tag{23}$$

where w_j are constants, and vectors $\boldsymbol{K}_j^{(i)}$ are as follows:

$$\boldsymbol{K}_j^{(i)} = h_i \boldsymbol{F}\left(\boldsymbol{X}_i + \sum_{l=1}^{m} a_{jl} \boldsymbol{K}_l^{(i)} t_i + c_j h_i\right), \tag{24}$$

where $h_i = t_{i+1} - t_i$ for $j = 1, \ldots, m$ and $c_j = \sum_{l=1}^{m} a_{jl}$.

For implicit m-stages Runge–Kutta methods can be chosen for some nodes $c_1, c_2, \ldots, c_m$, or those can be derived by high order approximation algorithms. It is well-known, that the highest order quadrature constitutes the Gaussian quadrature. Therefore, it is convenient to choose the nodes $c_1, c_2, \ldots, c_m$ since they are roots of a high-order quadrature. The paper presents some test methods based on Gauss–Legendre, Radau, and Lobatto quadrature approximations of the orders $2m$, $2m - 1$, and $2m - 2$, respectively. It can be proved that the implicit Runge–Kutta methods mentioned are A-stable, and are thus are most appropriate for the solution of stiff differential equations [1–4, 6, 16–18].

For the implicit Runge–Kutta algorithms there are derived the so-called embedded formulas [5, 6] that enable local error monitoring. The authors elaborated a numerical library for the C# language [1], which contains all implementations of the methods mentioned. Moreover, the Jacques J.B. de Swart and Gustaf Soderlind idea of integration error estimation is adopted [7]. This idea defines the error vector of i-th iteration as a difference between solution $\boldsymbol{X}_{i+1}$ and approximation $\widetilde{X}_{i+1}^{(1)}$:

$$\boldsymbol{E}_i = \boldsymbol{E}_i(t_i + h_i h_i)\boldsymbol{X}_{i+1} - \widetilde{X}_{i+1}^{(1)}. \tag{25}$$

The error can be written in the form of [1, 6]:

$$\boldsymbol{E}_i(t_i + h_i h_i) = [1 - \gamma h_i \boldsymbol{J}(\boldsymbol{X}_{i+1} t_i + h_i)]^{-1} \left[\sum_{j=0}^{m} e_j \boldsymbol{K}_j^{(i)} - \gamma h_i \boldsymbol{F}(\boldsymbol{X}_{i+1}, t_i + h_i)\right], \tag{26}$$

where $\boldsymbol{J}(\boldsymbol{X},t)$ is the Jacobi matrix for the vector function $\boldsymbol{F}(\boldsymbol{X},t)$, and

$$e_j = \begin{cases} -\widetilde{w}_0 & \text{for } j=0 \\ -\widetilde{w}_0 v_{j1} + \gamma p_j & \text{for } j=1,2,...,m \end{cases}, \quad p_i = \sum_{j=1}^{m} v_{ij},$$

are elements of the inverse of Vandermonde's matrix $[v_{ij}] = \boldsymbol{U}^{-1}$, where $\boldsymbol{U} = [(c_j)^{i-1}]$.

It is proved [5] that for the stability of the embedded method the following condition is necessary:

$$|\widetilde{w}_0/\gamma| < 1. \tag{27}$$

Theoretical investigations [7] and our own experimental tests indicate that the stability area for the embedded method for parameters $|\widetilde{w}_0/\gamma| = 0,067$, $\widetilde{w}_0 = 0.01$ is very close to the stability area of implicit Runge–Kutta methods. The numerical library elaborated is applied for designing objected-oriented programming to approach transient states of work of the transformer in a no-load work state.

4. Numerical example

For example, for testing the algorithm the following data for a three-phase transformer were chosen as shown in Table 1.

For example, three-phase transformer electrical steel sheets are chosen as the type Power Core H 105-30 ThyssenKrupp Elektrical Steel (Table 2).

The source voltages are sine varying of angular frequency $\omega = 2\pi f$ and are given arbitrary line-to-line voltage modules E_{12}, E_{23}, E_{31}, and phase for one of these voltages. The next two voltage phases result from the voltages triangle shown in Fig. 3. In Fig. 3 the complex voltage $\underline{E}_{23}$ is assumed as follows, $\underline{E}_{23} = \mathrm{j}E_{23}$.

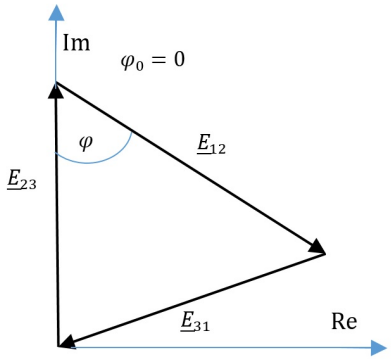

Fig. 3. Complex voltages diagram

Other effective complex values, i.e. their phases, result from the geometry of the triangle on Fig. 3.

$$\underline{E}_{12} = E_{12}\sin(\varphi) - \mathrm{j}\alpha, \tag{28}$$

where

$$\alpha = E_{12}\cos\varphi = \frac{E_{12}^2 + E_{23}^2 - E_{31}^2}{2E_{23}}, \tag{29}$$

$$\varphi = a\cos\left(\frac{\alpha}{E_{12}}\right). \tag{30}$$

Table 1. Transformer model parameters

Primary winding nominal voltage U_{ng} [V]	3 637
Secondary winding nominal voltage U_{nd} [V]	156
Primary winding nominal current I_{ng} [A]	1 100
Coil number of high voltage winding z_g	93
Winding power losses ΔP_{Cu} [kW]	36
Core power losses ΔP_{Fe} [kW]	11
Short-cut voltage u_{zw} [%]	5
Core cross-section S_{Fe} [m^2]	0.110565
Column length l_{Fe2} [m]	1.4
Yoke length l_{Fe1} [m]	0.76
Source line (line-to-line) voltage E 12 [V]: E_{21} [V], E_{12} [V]	6 000
Source line voltage E_{23} [V]	6 000
Source line voltage E_{31} [V]	6 000
Initial phase φ [deg]	0
Frequency f [Hz]	50
Equivalent resistance of line and source R_s [Ω]	0.040
Equivalent reactance of line and source X_s [Ω]	0.100

Table 2. Coefficient for curve $H(B)$ approximation for transformer core type Power Core H 105-30

i	a_i	i	a_i
1	29.9624271037522	7	1516.77585894405
2	–76.4912078883278	8	–630.577358829122
3	420.867774746849	9	160.397849549712
4	–1 274.37623231261	10	–22.7840824031901
5	2 196.27285444425	11	1.38472183966324
6	–2 301.93260519503		

Complex RMS voltages $\underline{E}_{23}$, $\underline{E}_{12}$ enable the complex RMS voltage $\underline{E}_{31}$ to be determined as follows:

$$\underline{E}_{31} = -\underline{E}_{12} - \underline{E}_{23}. \tag{31}$$

Complex RMS voltages $\underline{E}_{12}$, $\underline{E}_{23}$, $\underline{E}_{31}$ lead to cosine instantaneous voltages e.g.

$$e_{12}^{(s)}(t) = \sqrt{2}\left|\underline{E}_{12}\right| \cos\left(\omega t + \arg(\underline{E}_{12}) + \varphi_0\right). \tag{32}$$

The source voltage functions (32) force currents in transformer windings and are put into (21) and (22). The initial phase φ_0 is arbitrarily chosen and this gives insight into the influence on transient states of the initial time point $t = 0$. For the angle, $\varphi_0 = 0$ the phases of line-to-line voltages are shown in Fig. 3. To solve the equations of state (18) and (22), the initial conditions for the state vector are also necessary.

$$\boldsymbol{X} = [x_1(t), x_2(t), x_3(t), x_4(t)]^T = [i_1^{(g)}(t), i_2^{(g)}(t), \Psi_1(t), \Psi_2(t)]^T. \tag{33}$$

While for currents $i_1^{(g)}(t), i_2^{(g)}(t)$ the assumption of zero initial conditions is obvious from the point of view of tests when switching the voltage to the transformer at idle, the initial conditions for coupled magnetic fluxes $\Psi_1(t)$, $\Psi_2(t)$ should result from residual magnetism after the last transformer was switched off from the network. To show the influence of transformer switching currents from residual magnetism, a computational experiment was first carried out in which all initial conditions and thus fluxes were assumed to be zero. This solution is given in Fig. 4(a).

Figure 4(a) shows the solution of state variables $\Psi_k(t)$, $i_k^{(g)}(t)$ for $k = 1, 2, 3$ received from solutions of the differential sets (18) and (22) for two time periods $2T = 2/f$ of source voltage at at initial phase $\varphi_0 = 0$ with an automatically chosen integration step for a given absolute error of value $\varepsilon_a = 1e-7$ and relative error of value $\varepsilon_w = 1e-11$. The currents $i_k^{(g)}(t)$ for $k = 1, 2, 3$ presented take forms of impulses which gradually decrease.

To show the range of stiffness of the system of equations, we take into account, for example, phase 3 for the waveforms from Fig. 4(a). Starting from zero initial conditions, the magnetic flux associated with z_g turns $\Psi_3(t)$ slowly increases. This is accompanied by a slight increase in current $i_3^{(g)}(t)$ from zero to several amperes not visible in the figure in the range from zero to 5 ms. However, this current generates a flow generating the combined flux $\Psi_3(t)$, the derivative of which is the electromotive force $\mathrm{d}\Psi_3(t)/\mathrm{d}t$ induced in the coil of the upper side not much different from the phase voltage of the transformer. After 5 milliseconds of growth, the associated flux $\Psi_3(t)$ causes a gradual saturation of magnetic induction in the core, which with a further increase in current $i_3^{(g)}(t)$ gives a slight increase in the flux, which after some time reaches its maximum. The derivative of this flux, i.e. the electromotive force induced in the coil, decreases rapidly in this time interval, which causes a sharp increase in the current $i_3^{(g)}(t)$, which reaches its maximum at the moment of passage of the flux $\Psi_3(t)$, through the maximum.

Figure 4(b) and Fig. 4(c) give the solution of the state variables $\Psi_1(t), \Psi_2(t), \Psi_3(t)$, $i_1^{(g)}(t)$, $i_2^{(g)}(t)$, $i_3^{(g)}(t)$ from the solution of the system of differential Eqs. (18) and (22) in the integration interval of two periods of supply voltage with the initial phase of voltage $\varphi_0 = 0$ for a given residual magnetism respectively $B_1 = 0.2T$, $B_2 = -0.4T$, $B_3 = 0.2T$, and $B_1 = 0.4T$, $B_2 = -0.8T$, $B_3 = 0.4T$. The second residual magnetism dataset is twice as large as the first. In this set, the

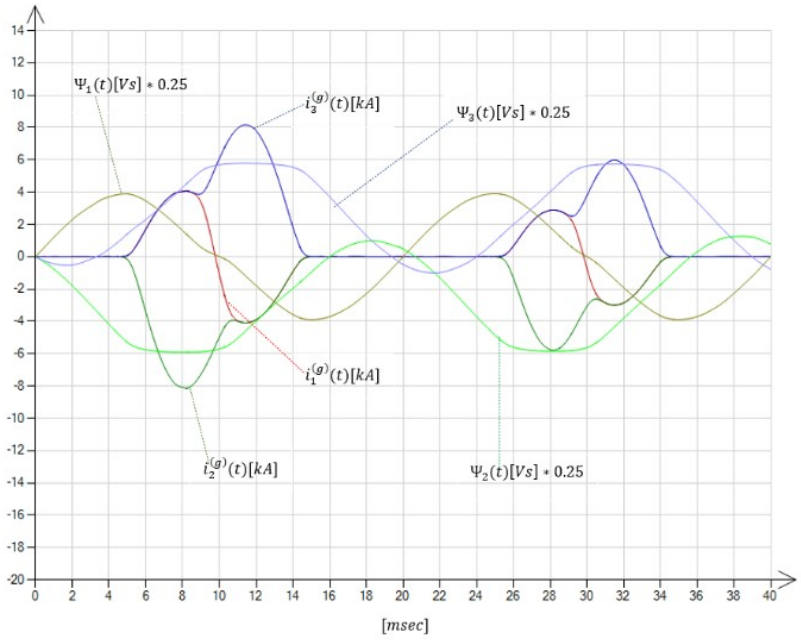

(a) Presentation of chosen variables of the transformer with zero initial phase $\varphi_0 = 0$ and zero residual magnetism

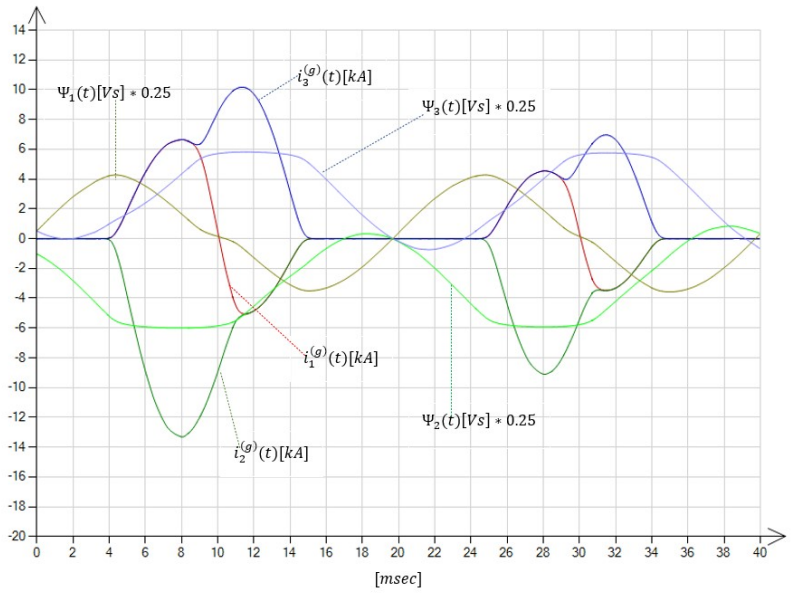

(b) Presentation of chosen variables of the transformer with zero initial phase $\varphi_0 = 0$ and with residual magnetism $B_1 = 0.2T$, $B_2 = -0.4T$, $B_3 = 0.2T$

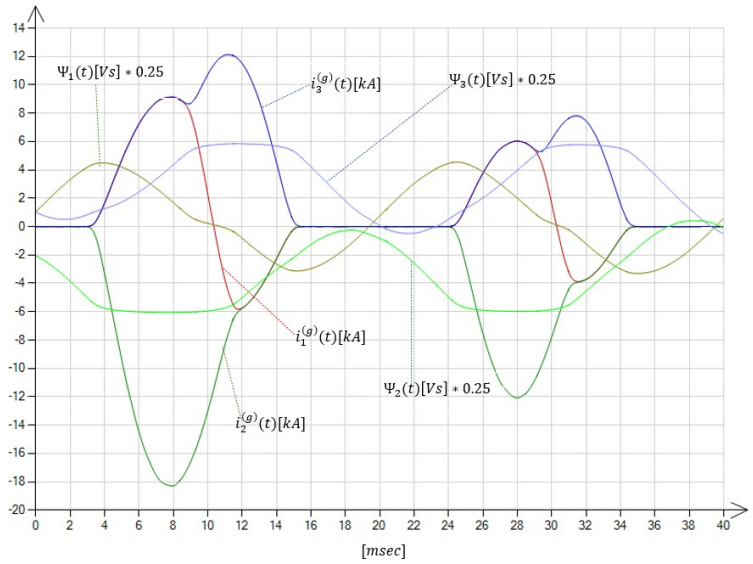

(c) Presentation of chosen variables of the transformer with zero initial phase $\varphi_0 = 0$ and with residual magnetism $B_1 = 0.4T$, $B_2 = -0.8T$, $B_3 = 0.4T$

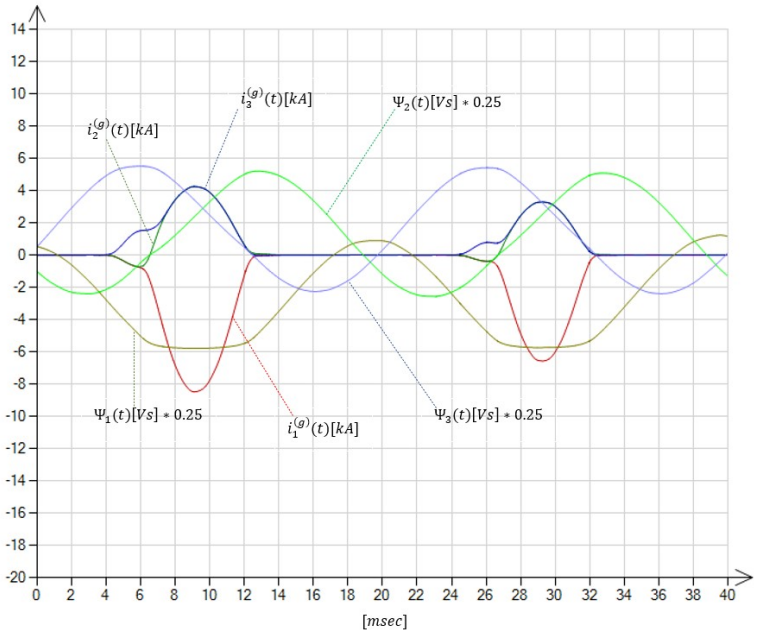

(d) Presentation of chosen variables of the transformer with zero initial phase $\varphi_0 = 100$ and with residual magnetism $B_1 = 0.2T$, $B_2 = -0.4T$, $B_3 = 0.2T$

Fig. 4. Presentation of chosen variables of the transformer

maximum values of phase currents existing in the first integration period are proportionally greater in relation to the data from the first set.

Subsequently, a numerical experiment was carried out, assuming residual magnetism in the form of $B_1 = 0.2T$, $B_2 = -0.4T$, $B_3 = 0.2T$ as in the experiment shown in Fig. 4(b), while the initial phase of supply voltages was assumed $\varphi_0 = 100$ (Fig. 4(d)). In this example, significant reductions in the value of current pulses can be observed, which can be explained by the initial demagnetization of residual magnetism by appropriate voltage forcing in a given initial phase.

The investigations of the transient state of work at zero initial conditions and the automatically chosen integration step are provided by applying different methods of quadrature approximation such as Gauss–Legendre, Radau, and Lobatto. Table 3 presents the number of iterations necessary for integrations for five time periods of voltage source which are presented in Fig. 4(a). The minimal number of iterations needs methods Radau IIA and Lobatto IIIC. The total numerical effort is minimal for the Lobatto IIIC method.

Table 3. Coefficient for curve $H(B)$ approximation for transformer core type Power Core H 105-30

Method name	Step number	Method order	Iterations number	Time [ms]
Gauss–Legendre	5	10	1 127	1 531
Radau IA	5	9	2 005	2 830
Radau IIA	5	9	438	1 653
Lobatto IIIC	5	8	444	1 241

The stiffer the differential Eqs. (18) and (22), the higher the current impulses of primary windings $i_k^{(g)}(t)$ will be (Fig. 5). The maximal impulse values also depend on the initial phase φ_0 of source voltage (28) and may exhibit some minimal and maximal values. The solutions are obtained for initial angles φ_0 from 0°to 180°for searching the maximal value of all current impulses

$$\max_t \left\{ \left| i_1^{(g)}(t) \right|, \left| i_2^{(g)}(t) \right|, \left| i_3^{(g)}(t) \right| \right\},$$

during the startup of the transformer at a no-load state of work. The numerical analysis investigations with zero residual magnetism show that the greater the voltage per coil number, the greater the current impulses will be, as is shown in Fig. 5. The ratio voltage per coil number is important for the design process because it is decisive for saturation effects. Moreover, the greater the saturation effect, the greater the current impulses during the startup of the transformer. The maximal current impulses at the startup of the transformer also depend on source resistances (Fig. 6).

However, the question arises what effect the residual magnetism in the transformer has on these pulses, which can be taken into account in the given model in the form of initial conditions for conjugated fluxes $\Psi_1(t)$, $\Psi_2(t)$. These conditions depend on the time moment of a given period of network voltage from which the short process of switching off the transformer power supply begins. In the process of extinguishing current and flux in transformer columns, at any moment of this process, Kirchhoff's first law for fluxes occurs (7). When the current reaches zero

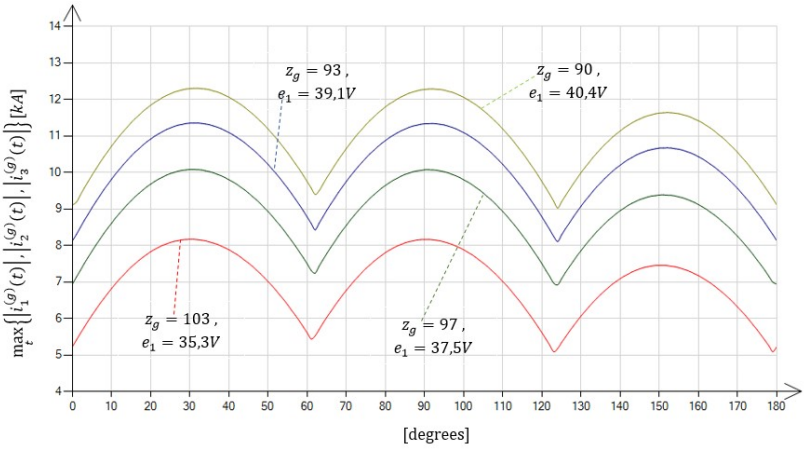

Fig. 5. Maximal inrush current at startup vs. input voltage initial angle with zero residual magnetism

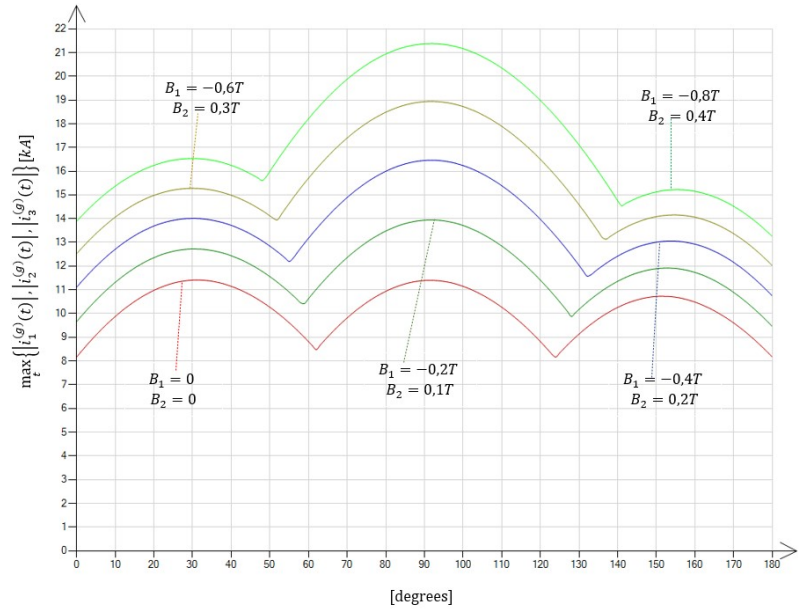

Fig. 6. Maximal inrush current at startup vs. input voltage initial angle for different residual magnetism value

values after some time, the magnetic fluxes due to residual magnetism will be different from zero but will also meet the conditio $\Psi_1(t_0) + \Psi_2(t_0) + \Psi_3(t_0) = 0$. Since the state variables are $\Psi_1(t_0)$, $\Psi_2(t_0)$, the third condition for $\Psi_3(t_0)$ is automatically satisfied because the above equation is included in the construction of the state equations of the modeled transformer. Since the initial conditions $\Psi_1(t_0)$, $\Psi_2(t_0)$ depend on the time moment of a certain period in which the process

of extinguishing transformer streams began, it is proposed in numerical experiments to introduce a certain parameter φ_B to set these quantities:

$$B_i = B_{\text{res}i}\cos\left(\varphi_B + (i-1)\frac{2\pi}{3}\right)\Psi_1(t_0) = B_1 S_{\text{Fe}} z_g \Psi_2(t_0) = B_2 S_{\text{Fe}} z_g\,, \tag{34}$$

were $B_{\text{res}i}$ is the maximum residual magnetism value for transformer sheets.

Figure 6 shows the results of calculations of the maximum values of currents for $z_g = 93$ and when switching on the transformer voltage depending on the initial phase of these voltages for different values of residual magnetism $B_1 = B_{\text{res}i}\cos\pi B_2 = B_{\text{res}i}\cos\left(\varphi_B + \frac{2\pi}{3}\right)$, taking as $B_{\text{res}i}$ the values of 0 T respectively; 0.2 T; 0.4 T; 0.6 T; 0.8 T. It can be noted that for the selected proportion of residual magnetism in individual columns of the transformer core, the maximum values of the switching currents increase proportionally with an increase $B_{\text{res}i}$ from 0 to 0.8 T for all values of the initial phase of switching on the voltage. This is shown exactly in Fig. 7 where it can be seen that for selected initial phases of switching on the voltage, the maximum values of currents increasing linearly starting from the zero value of residual magnetism. Such a regularity is paid attention to in the works [10] and [11].

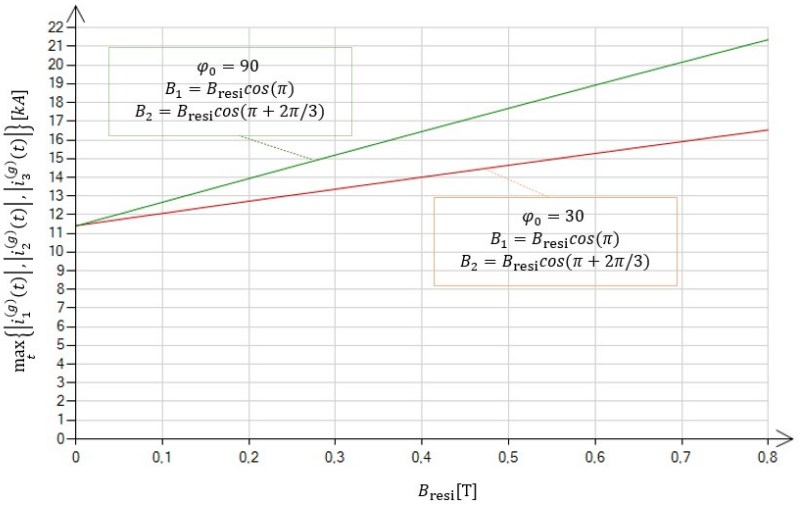

Fig. 7. Maximal inrush current at startup vs. input voltage initial angle and differential φ_0 value

The characteristics of the distribution of the maximum values of current pulses when the transformer voltage is switched on as a function of the initial phase of this voltage depend not only on the proportion of residual magnetism in individual columns of the transformer but also on their level. It can be noted that for the selected proportion of residual magnetism in the individual columns of the transformer core, the maximum values of the switching currents increase proportionally with an increase $B_{\text{res}i}$ from 0 to 0.8 T (Fig. 8) for all values of the initial phase of switching on voltages less than $\varphi_0 < 90$. For all initial phase greather then $\varphi_0 > 90$ smaller values of current pulses are observed compared to the case of the existence of zero

residual magnetism. Figure 9 shows that for the selected initial phase of switching on the voltage $\varphi_0 = 50$, the maximum values of currents increasing linearly starting from the zero value of residual magnetism. If, on the other hand, the initial phase $\varphi_0 = 110$, a decrease in the values of the maximum current pulses is observed, starting from the zero value of residual magnetism (Fig. 9). Such a regularity is paid attention to also in the works [10] and [11].

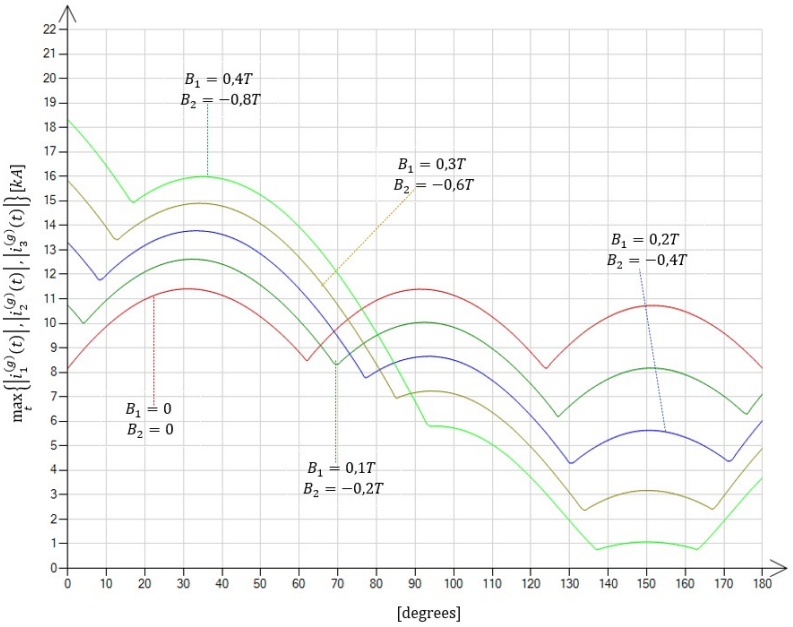

Fig. 8. Maximal inrush current at startup vs. input voltage initial angle for different residual magnetism value

Numerical experiments show that in each case of switching on the transformer voltage in the idle state, there is freedom of proportions of residual magnetism and their values, as well as freedom of the moment of switching on this voltage. This creates a great variety of responses in the form of current pulses. The maximal current impulses at the startup of the transformer also depend on source resistances (Fig. 10).

The values of current pulses depend not only on residual magnetism and the initial phase of the supply voltage, but also on the resistance of the windings R_g as well as on the equivalent resistance of the R_s mains supply. For example, Fig. 6 shows the distribution of maximum values of current pulses when switching the supply voltage to a three-phase transformer not loaded at zero residual magnetism, depending on the replacement resistance of the power source. The implementation of the integration process in the first period of the supply voltage despite the rigidity of its differential Eqs. (18) and (22) (see the waveforms in Figs. 4(a)–4(d)) does not pose any problems due to the absolute stability of the implicit methods used in the calculation process. The own numerical library [1] used for the implementation of calculations is additionally equipped with methods that record the error estimated both in the calculation process with a fixed integration step and in its automatic selection.

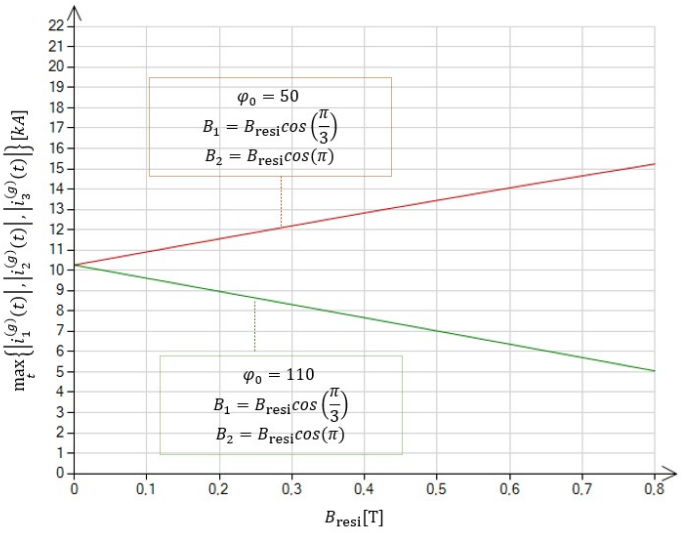

Fig. 9. Maximal inrush current at startup vs. input voltage initial angle and differential φ_0 value

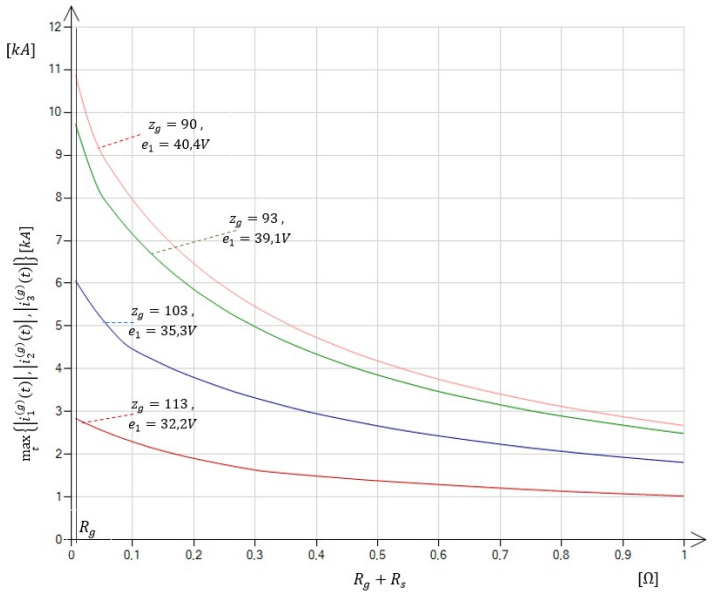

Fig. 10. Maximal current impulses at transformer switch on vs. source resistance

Figure 11 shows the decimal logarithm of the estimated error vector norm for the examples presented in Fig. 4(a). In particular, the numerical calculations have been performed with automatically chosen integration steps for given absolute error of the value absolute error $\varepsilon_a = 1e-7$

and relative error of value $\varepsilon_w = 1e-11$. Figure 11 confirms that the applied algorithm always keeps the absolute error limit. In conclusion, it could be stated that for the transient and steady states investigated of the three-phase transformer the applied algorithm always satisfies the given absolute error.

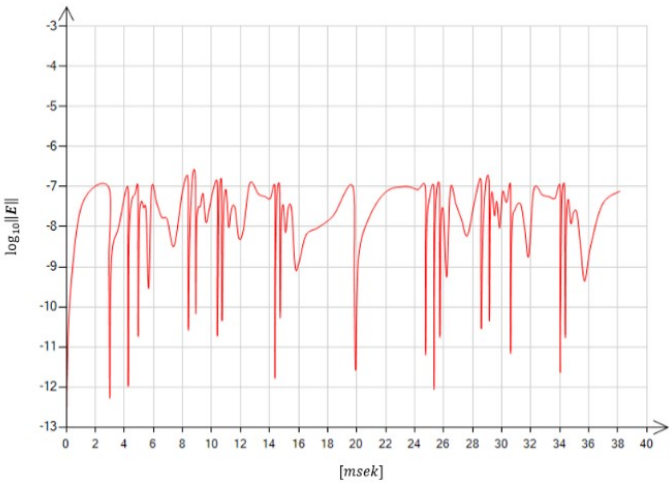

Fig. 11. Decimal logarithm of estimated error (21) norm vs. time for solutions presented in Fig. 4(a)

5. Steady-state analysis of a three-phase nonlinear transformer

The important problem is to reach steady state variable values without integrating differential Eqs. (18) and (22) over the long-time domain from zero initial conditions. As mentioned above, implicit Runge–Kutta algorithms enable stable integration of a stiff differential equation set, but this requires a significant numerical effort. It is reasonable to try to find some nonzero initial conditions which are close to steady state variable values. For such initial conditions, the steady-state solutions can be derived by means of integrations over only a few time periods of the source voltage. The approximation of such initial conditions can be obtained while assuming the linearity of the magnetizing curve of the transformer core. Based on this assumption the differential Eqs. (18) and (22) are linear and have analytical solutions. In this case, the phase plane shows limit cycles in the shape of eclipses. Moreover, to find analytical solutions for the steady state of a linear transformer the complex method of circuit analysis can be applied.

The process of algorithm design starts with the assumption that the magnetizing curve is linear. The magnetic voltage drops for transformer branches ($k = 1, 2, 3$) and is approximated in the following linear formula:

$$U_{\mu,k}(\Psi_k(t)) = h_{\mathrm{Fe},k} H\left(\frac{\Psi_k(t)}{z_g S_{\mathrm{Fe}}}\right) = \frac{h_{\mathrm{Fe},k}}{z_g \mu_p S_{\mathrm{Fe}}}\Psi_k(t) = \frac{R_{\mu,k}}{z_g}\Psi_k(t), \tag{35}$$

where $\mu_p = B_p/H_p$ magnetic permeability for linear subinterval of magnetizing curve, $R_{\mu,k} = h_{\mathrm{Fe},k}/(\mu_p S_{\mathrm{Fe}})$ approximated magnetic permeance of magnetic circuit phase number k.

Linear approximation (33) of the magnetization curve is applied to Eq. (14), and taking into account (18) a linear differential equation set is obtained, which can be analytically solved for sinusoidal steady state based on a complex steady state in the algebraic form of

$$\begin{bmatrix} \underline{Z}_Z & -\underline{Z}_Z & 0 & \mathrm{j}\omega & \mathrm{j}\omega & 0 \\ 0 & \underline{Z}_Z & -\underline{Z}_Z & 0 & \mathrm{j}\omega & -\mathrm{j}\omega \\ 1 & 1 & 1 & 0 & 0 & 0 \\ 1 & -1 & 0 & -\underline{Z}_{fe,1} & \underline{Z}_{fe,2} & 0 \\ 0 & 1 & -1 & 0 & -\underline{Z}_{fe,2} & \underline{Z}_{fe,3} \\ 0 & 0 & 0 & 1 & 1 & 1 \end{bmatrix} \begin{bmatrix} \underline{I}_1^{(g)} \\ \underline{I}_2^{(g)} \\ \underline{I}_3^{(g)} \\ \underline{\Psi}_1 \\ \underline{\Psi}_2 \\ \underline{\Psi}_1 \end{bmatrix} = \begin{bmatrix} \underline{E}_{12}^{(g)} \\ \underline{E}_{23}^{(g)} \\ 0 \\ 0 \\ 0 \\ 0 \end{bmatrix}, \tag{36}$$

where $\underline{Z}_z = R_z + \mathrm{j}\omega L_z$, $\underline{Z}_{\mathrm{Fe},k} = R_{\mu k}/z_g^2 + \mathrm{j}\omega/R_{\mathrm{Fe},k}$, $\underline{E}_{12}^{(s)} = \sqrt{2}\underline{E}_{12}e^{\mathrm{j}\varphi_0}$, $\underline{E}_{23}^{(s)} = \sqrt{2}\underline{E}_{23}e^{\mathrm{j}\varphi_0}$.

The solutions of linear differential equation set (35) are denoted by $\underline{\Psi}_k$, $\underline{I}_k^{(g)}$ for $k = 1, 2, 3$. Equations (18) and (22) at steady state for cosine source voltages $\underline{E}_{12}^{(s)}$, $\underline{E}_{23}^{(s)}$ for linear approximation can be given as follows:

$$\begin{aligned} \widetilde{i}_k^{(g)}(t) &= \mathrm{Re}\left\{\underline{I}_k^{(g)} \exp(\mathrm{j}\omega t)\right\} = I_{m,k}^{(g)} \cos(\omega t + \beta_k), \\ \widetilde{\Psi}_k(t) &= \mathrm{Re}\left\{\underline{\Psi}_k \exp(\mathrm{j}\omega t)\right\} = \Psi_{m,k} \cos(\omega t + \beta_k). \end{aligned} \tag{37}$$

The phases of currents $\widetilde{i}_k^{(g)}(t)$ and flux linkages $\widetilde{\Psi}_k(t)$ for steady state are usually different $\alpha_k \neq \beta_k$, and thus in the phase plane, these complex vectors describe an ellipse during one period. For a nonlinear transformer core, the limit phase diagram will be different than that of an ellipse (i.e. oval) but relatively close to it. Based on this knowledge it is assumed that the initial conditions are equal to steady state solutions for a linear steady state of work, i.e. the initial conditions for (17) and (20) are as follows:

$$\begin{aligned} x_k(0) &= i_k^{(g)}(0) = \widetilde{i}_k^{(g)}(0) = \mathrm{Re}\left\{\underline{I}_k^{(g)}\right\}, \\ x_{k+2}(0) &= \Psi_k(0) = \widetilde{\Psi}_k(0) = \mathrm{Re}\left\{\underline{\Psi}_k^{(g)}\right\}, \end{aligned} \tag{38}$$

for $k = 1, 2$.

Numerical experiments confirm that the number of time periods of source voltages needed for the integration of equation sets (17) and (20) is relatively small. Steady-state detection can be provided by means of discrete Fourier transform [1, 3, 4, 22]. Zero (constant item) of the Fourier transform of state variables is evaluated based on one period of source voltage.

Based on the analysis carried out the following algorithm can be proposed:

1. Data introduction based on Tables 1 and 2.
2. Defining steady-state level $\varepsilon_{st} > 0$.
3. Formulation of differential sets of Eqs. (18) and (22).
4. Introduction of initial conditions (37) as solutions of algebraic equation set (36).

5. Choosing implicit Runge–Kutta method for integration of nonlinear differential equation sets (18) and (22).
6. Integration with an automatically chosen step over the time interval in which length is an integer multiple N_o of source voltage period.
7. Continuation of integration #6 with constant step and calculation of simple Fourier transformation coefficients of state variable.
8. If the module of zero coefficient (constant item) satisfies steady-state level ε_{st} then go to #9. If not go to #6 and continue the procedures.
9. Acquisition of state variables and output functions.
10. Graphical presentation of results.

In the algorithm presented above the numerical program in C# language has been elaborated. The program applies the design of the authors' numerical library [1–3], which contains the implementation of implicit Runge–Kutta methods based on Gauss–Legendre, Radau, and Lobatto approximation quadratures. For example, a three-phase transformer with data presented in Tables 1 and 2 was considered. With initial conditions (36) and integration over the interval of $N_o = 15$ time periods of source voltage, a steady state is reached. The limit cycle for a nonlinear transformer is presented in Fig. 12. Moreover, Fig. 12 also shows the limit cycle for the linear model of the transformer where initial condition (35) is drawn as one point on this limit cycle.

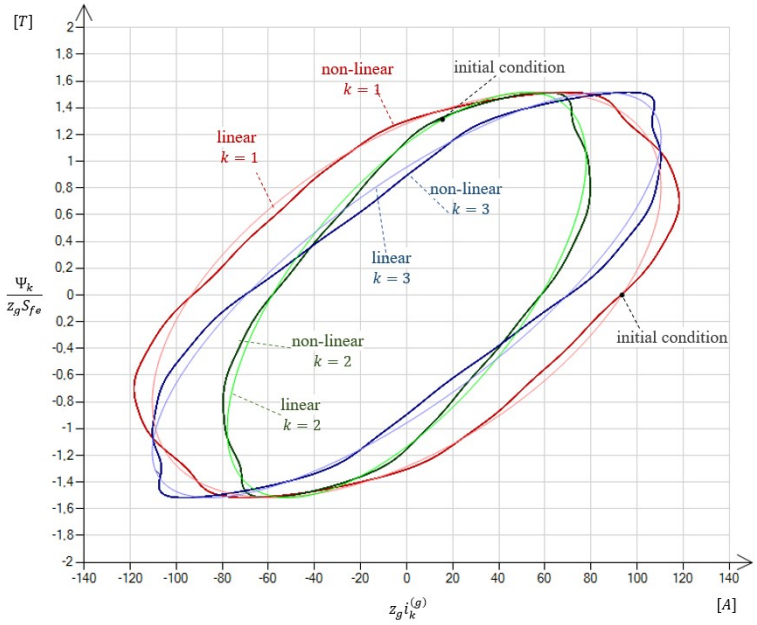

Fig. 12. Phase plane for steady state for a linear and nonlinear model of a three-phase transformer

The integration process was carried out with the help of Radau IIA and Lobatto IIIC methods applying automatically chosen steps for the required absolute error $\varepsilon_a = 1e{-}7$ and relative error of value $\varepsilon_w = 1e{-}11$.

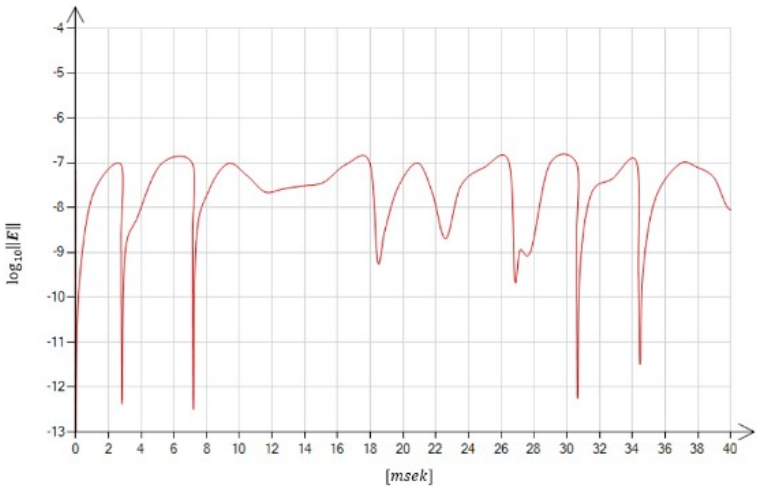

Fig. 13. Decimal logarithm of estimated error (21) norm vs. time for solutions presented in Fig. 4(a)

The results in Fig. 12 prove that the applied algorithms satisfy the required absolute error. The numerical calculations were performed for a few orders of Radau IIA and Lobatto IIIC methods. The number of iterations, calculation times, and algorithm parameters are set in Table 4. Radau IIA and Lobatto IIIC methods have a very similar number of iterations needed for satisfying the required absolute error with automatically chosen steps. However, the Lobatto IIIC method needs lower total time for calculations such that the numerical effort is lower than for the Radau IIA method.

Table 4. Comparison of Radau IIA and Lobatto IIIC methods

Radau IIA method ($\varepsilon_a = 1e-7, \varepsilon_w = 1e-11$)				**Lobatto IIIC method** ($\varepsilon_a = 1e-7, \varepsilon_w = 1e-11$)			
Steps number	**Order**	**Number of iterations**	**Time [ms]**	**Steps number**	**Order**	**Number of iterations**	**Time [ms]**
3	5	635	308	3	4	819	503
4	7	464	785	4	6	392	426
5	9	416	1 330	5	8	362	494
6	11	394	1 801	6	10	289	517
7	13	312	1 871	7	12	229	682

The algorithm for steady-state nonlinear transformer determination can be used for defining the nominal state of work and pointing out the loci on a magnetizing curve in order to reduce higher harmonic content. For this purpose, a discrete Fourier transform is used and applied for data acquisition during one source voltage time period of integration with constant step. For the

steady state of the nonlinear transformer higher harmonics for each locus for the no-load state of work can be determined. For example, for integrations depicted in Fig. 11, a higher harmonics content for primary winding no-load current is presented in Fig. 14 and Fig. 15 [5–7, 23]. The asymmetry of no-load phases A, B, and C currents' results from the asymmetry of the three-phase transformer magnetic circuit which is accounted for in the model by assuming different magnetic circuit lengths for transformer phases.

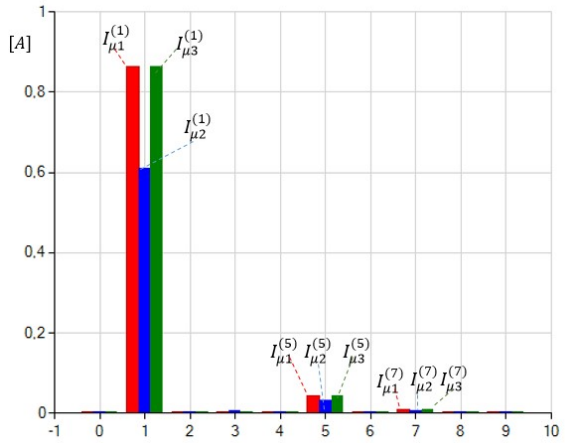

Fig. 14. Higher harmonics of no-load current of primary winding at line-to-line voltage 6 kV

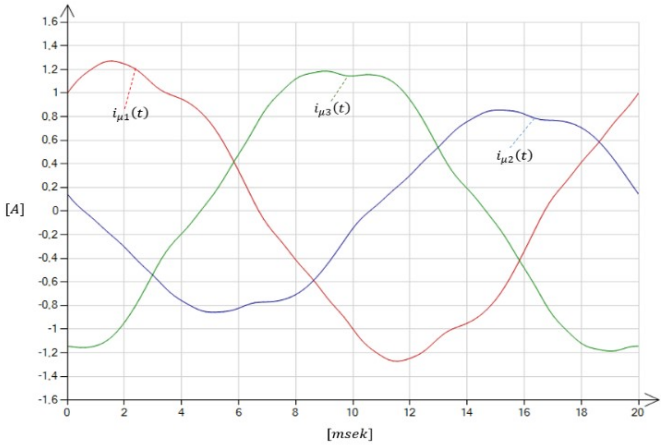

Fig. 15. Waveform deformation of no-load currents of primary windings at line-to-line voltage 6 kV

Moreover, the proposed algorithm and library are also used to evaluate higher harmonics ($h = 1, 3, 5, 7, \ldots$) of magnetizing currents $I_{\mu1}^{(h)}$, $I_{\mu2}^{(h)}$ and $I_{\mu3}^{(h)}$, such as for different primary

winding coil numbers z_g for source line-to-line voltages 6 kV. Additionally, the results are presented as a ratio to voltage per one coil.

Tracking of higher harmonic values helps in designing the proper locus of a three-phase transformer for a nominal state of work. Table 5 indicates that when a certain voltage value is reached then harmonic values rise significantly higher.

Table 5. Magnetizing current RMS and higher harmonics values for different transformer loci at constant primary voltage per coil

Parameter	**Phase A (k = 1)**	**Phase B (k = 2)**	**Phase C (k = 3)**
e_1 [V]	39.11	39.11	39.11
$I_{\mu k}$ [A]	0.8652	0.6104	0.8651
$I_{\mu k}^{(1)}$ [A]	0.8639	0.6095	0.8639
$I_{\mu k}^{(3)}$ [A]	0.0035	0.0070	0.0035
$I_{\mu k}^{(5)}$ [A]	0.0446	0.0314	0.0446
$I_{\mu k}^{(7)}$ [A]	0.0104	0.0073	0.0104
$I_{\mu k}^{(0)}$ [A]	0.000000998	0.000000281	0.000000716

6. Conclusions

Technological innovation of a transformer core, such as that of electrical sheets, leads to a significant increase in magnetic flux density. This ensures the decrease of the transformers' magnetic circuit dimensions. On the other hand, the magnetizing currents increase at transients and often contain higher harmonics during work at a steady state. However, the mathematical consequence is that the differential state equation set becomes stiff. In order to solve the differential state equation set for transient states of a three-phase transformer, Runge–Kutta with Gauss–Legendre, Radau, and Lobatto methods with maximal order quadrature formulas were applied. Based on the authors' numerical library [1] is elaborated in C# program language, objective oriented. For example, the algorithms and program for a three-phase transformer at a no-load state of work were applied. The results presented can improve the design process of three-phase transformers in choosing the nominal state of work, higher harmonics content, peak current values, and transient state analysis. The authors emphasize that the transient states' analyses of nonlinear three-phase transformers at a no-load state of work are important for investigating their maintenance and reliability, as well as for power-system automation work.

References

[1] Baron B., Kolańska-Płuska J., *Numerical methods of solving ordinary differential equations in C#*, Politechnika Opolska Publisher (in Polish), ISBN 978 83 65235 30 5 (2015).

[2] Baron B., Kolańska-Płuska J., Waindok A., Kraszewski T., Kawala-Sterniuk A., *Application of Runge–Kutta implicit methods for solving stiff non-linear differential equations of a single-phase transformer*

model in the no-load state. Innovation Management and information Technology impact on Global Economy in the Era of Pandemic, Proceedings of the 37th International Business Information Management Association Conference (IBIMA), ISBN-13: 978-1-4200-0760-2 (Ebook-PDF), pp. 8071–8087, https://ibima.org/accepted-paper/application-of-runge-kuttas-implicit-methods-for-solving-stiff-non-linear-differential-equations-of-a-single-phase-transformer-model-in-the-no-load-state/ (2021).

[3] Baron B., Kolańska-Płuska J., Kraszewski T., *Application of Runge–Kutta implicit methods to solve the rigid differential equations of a single-phase idle transformer model*, Politechnika Poznańska, Zeszyty Naukowe nr 100 (in Polish), Electrical Engineering (2019), DOI: 10.21008/j.1897-0737.2019.100.0007.

[4] Dos Passos W., *Numerical Methods Algorithms and Tools in C#*, CRC Press, Taylor & Francis Group LLC, Boca Raton London New York, ISBN-13: 978-1-4200-0760-2, Ebook-PDF (2010), https://www.routledge.com/Numerical-Methods-Algorithms-and-Tools-in-C/Passos/p/book/9781439859070.

[5] Dekker K., Verwer J.G., *Stability of Runge–Kutta methods for stiff nonlinear differential equations*, Elsevier Science Publishers B.V., North-Holland Amsterdam-New York – Oxford (1984), DOI: 10.1002/zamm.19870670128.

[6] Hairer E., Wanner G., *Solving Ordinary Differential Equations II: Stiff and Differential-algebraic Problems*, 2nd revised ed., Springer, Berlin (2010) https://rd.springer.com/content/pdf/bfm:978-3-642-05221-7/1.pdf.

[7] de Swart J.J.B., Soederlind G., *On the construction of error estimators for implicit Runge–Kutta methods*, Journal of Computational and Applied Mathematics 86, pp. 347–358 (1997), DOI: 10.1016/S0377-0427(97)00166-0.

[8] Dombek G., Nadolny Z., *Liquid kind, temperature, moisture, and ageing as an operating parameters conditioning reliability of transformer cooling system*, Eksploatacja i Niezawodność – Maintenance and Reliability, vol. 18, no. 3, pp. 413–417 (2018), DOI: 10.17531/ein.2016.3.13.

[9] Gutten M., Korenciak D., Kucera M., Sebok M., Opielak M., Zukowski P., Koltunowicz T., *Maintenance diagnostics of transformers considering the influence of short-circuit currents during operation*, Eksploatacja i Niezawodność – Maintenance and Reliability, vol. 19, no. 3, pp. 459–466 (2017), DOI: 10.17531/ein.2017.3.17.

[10] Horiszny J., *Research of leakage magnetic field in deenergized transformer*, Compel – The international journal for computation and mathematics in electrical and electronic engineering, vol. 37, pp. 1657–1667 (2018), DOI: 10.1108/compel-01-2018-0040.

[11] Horiszny J., *Analysis and reduction of transformer inrush current*, Gdansk University of Technology, monograph 159 (in Polish) (2016).

[12] Pandey S.B., Lin C., *Estimation for a life model of transformer insulation under combined electrical and thermal stress*, IEEE Transactions on Reliability, vol. 41, no. 3, pp. 466–468 (1992), DOI: 10.1109/24.159823.

[13] Nicolet A., Delince F., *Implicit Runge–Kutta methods for transient magnetic field computation*, IEEE Trans. Magn., vol. 32, no. 3, pp. 1405–1408 (1996), DOI: 10.1109/20.497510.

[14] Noda T., Takenaka K., Inoue T., *Numerical integration by the 2-stage diagonally implicit Runge–Kutta method for electromagnetic transient simulations*, IEEE Trans. Power Del., vol. 24, no. 1, pp. 390–399 (2009), DOI: 10.1109/TPWRD.2008.923397.

[15] Pries J., Hoffmann H., *State Algorithms for Nonlinear Time-Periodic Magnetic Diffusion Problems Using Diagonally Implicit Runge–Kutta Methods*, Magnetics IEEE Transactions on, vol. 51, no. 4, pp. 1–12 (2015), DOI: 10.1109/TMAG.2014.2344005.

[16] Rosser J.B., *A Runge–Kutta for all seasons*, SIAM Rev., vol. 9, pp. 417–452 (1967), DOI: 10.1137/1009069.

[17] Wang X., Weile D.S., *Implicit Runge–Kutta methods for the discretization of time domain integral equations*, IEEE Trans. Antennas Propag., vol. 59, no. 12, pp. 4651–4663 (2011), DOI: 10.1109/TAP.2011.2165469.

[18] Noda T., Takenaka K., Inoue T., *Numerical Integration by the 2-Stage Diagonally Implicit Runge–Kutta Method for Electromagnetic Transient Simulations*, IEEE Transactions on Power Delivery, vol. 24, no. 1 (2009), DOI: 10.1109/TPWRD.2008.923397.

[19] Gołębiowski M., Mazur D., *Measurement and calculation of 3-column 15-winding autotransformer*, Archives of Electrical Engineering, vol. 60, no. 3, pp. 223–230 (2011), DOI: 10.2478/v10171-011-0021-8.

[20] Chraygane M., El Ghazal N., Fadel M., Bahani B., Belhaiba A., Ferfra M., Bassoui M., *Improved modeling of new three-phase high voltage transformer with magnetic shunts*, Archives of Electrical Engineering, vol. 64, no. 1, pp. 157–172 (2015), DOI: 10.1515/aee-2015-0014.

[21] Bavendiek G., Leuning N., Müller F., Schauerte B., Thul A., Hameyer K., *Magnetic anisotropy under arbitrary excitation in finite element models*, Archives of Electrical Engineering, vol. 68, no. 2, pp. 455–466 (2019), DOI: 10.24425/aee.2019.128280.

[22] Spałek D., *Two relations for generalized discrete Fourier transform coefficients*, Bulletin of the Polish Academy of Sciences: Technical Sciences, vol. 66, no. 3, pp. 275–281 (2018), DOI: 10.24425/123433.

[23] Spałek D., *Nonlinear magnetic circuit – self inductance definitions, passivity and waveforms distortion*, Bulletin of the Polish Academy of Sciences, Technical Sciences (2022), DOI: 10.24425/bpasts.2022.141003.